http://dx.doi.org/10.11142/jicems.2014.3.3.325
Journal of International Conference on Electrical Machines and Systems vol. 3, no. 3, pp. 325~330, 2014

Robust and Efficient 3D Model of an Electromagnetic Induction (EMI) Sensor

Chafic Abu Antoun* and Yves Perriard**

Abstract - Eddy current induction is used in a wide range of electronic devices, for example in detection sensors. Due to the advances in computer hardware and software, the need for 3D computation and system comprehension is a requirement to develop and optimize such devices nowadays. Pure theoretical models are mostly limited to special cases. On the other hand, the classical use of commercial Finite Element (FE) electromagnetic 3D models is not computationally efficient and lacks modeling flexibility or robustness. The proposed approach focuses on: (1) implementing theoretical formulations in 3D (FE) model of a detection device as well as (2) an automatic Volumetric Estimation Method (VEM) developed to selectively model the target finite elements. Due to these two approaches, this model is suitable for parametric studies and optimization of the number, location, shape, and size of PCB receivers in order to get the desired target discrimination information preserving high accuracy with tenfold reduction in computation time compared to commercial FE software.

Keywords: Volumetric Estimation Method, electronic devices, finite elements

1. Introduction

The basic components of a detection system, as sketched in Fig. 1, are the physical method, target and sensor. For magnetically permeable and electrically conductive targets, like steel and copper, the EMI physical method is one of the best candidates for such detection devices due to its low cost [2], low electronics requirements [9], relative indifference to environmental effects [6], and low or even no requirement for certification of devices or users. Referring to Fig. 1, a coil sender, excited with time varying current, creates a magnetic field that in turn creates eddy currents in hidden targets. The eddy currents will in turn create a magnetic field that induces a voltage signal in the receiver coil or sensor. This induced voltage, when analyzed, can provide the required information about the target. Higher precision, greater accuracy and more information about hidden targets like their material, shape, and orientation [8] are basic industrial requirements. To be able to meet these requirements, a verified practical system model is needed. Experiments have limitations due to noise at low signals and interferences as well as the difficulty of capturing physical effects, such as mutual inductance and eddy currents. Eddy currents cannot be measured

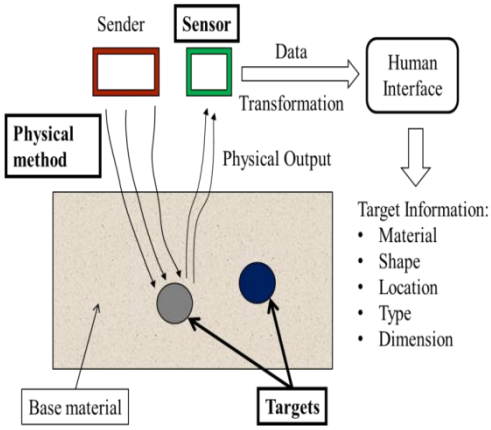

Fig. 1. Basics of a detection system: target, sensor, and physical method

or captured in reality. In contrast to experimental systems, 3D simulation models don't have such limitations, but rather other disadvantages like model flexibility and huge computation times. Theoretical models, on the other hand, exist only for the simplest shapes such as a permeable conductive spheroid or a sphere [3], [4].Many papers [1], [5], [7] contributed to modeling of such systems by using the advantage of the computational 3D capability and still

* Chafic Abu Antoun, IMT-LAI, Ecole Polytechnique Fédérale de Lausanne, Switzerland (EPFL), Chafic.abuantoun@epfl.ch

** Yves Perriard, IMT-LAI, Ecole Polytechnique Fédérale de Lausanne, Switzerland (EPFL), Yves.Perriard@EPFL.ch

Received 21 April 2014 ; Accepted 12 May 2014

implementing theoretical models where necessary to preserve the accuracy required and provide the robustness and fast computational time needed. Similarly, the current approach focuses on modeling a detection sensor, in this case, made of Printed Circuit Board (PCB) sender and receiver coils. The final model will be fast, robust and accurate enough to be used in optimization methods.

2. Fea Complete Simulation Model

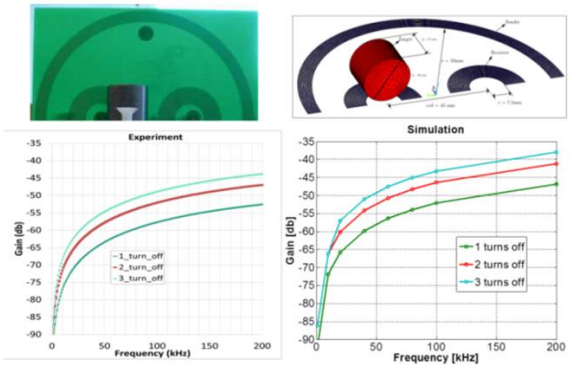

Fig. 2. Experiment (left) versus Simulation of the amplitude ratio of the receiver and sender

Complete 3D simulation model using commercial finite element software, ANSYS, is built up. A first step verification is performed to check if the sender and receivers are modeled correctly. Fig. 2 shows the experiment versus simulation results without any targets involved. If the sender is excited by a small current harmonic signal then the output is the induced voltage of all the coils. The two receivers were connected in series and were identical both by number of turns and by geometry. Theoretically a V_r=0V (-∞ dB) should be induced in the receiver if the target is absent.

In order to create non-symmetry in the system, some turns of 'only' one of the two receivers are then deactivated. Fig. 2 plots the results of both experiment and simulation for three wire eliminations consecutively. The simulation gives reasonable results and one can proceed further in the next step: to introduce a target with a certain shape, size, material and location. This complete, verified, 3D simulation model will be used as a reference that is compared to modified models described in the next sections.

$$\Phi = \oint \vec{A} dl \tag{1}$$

$$u = -\frac{d\Phi}{dt} \tag{2}$$

3. Line Receiver Model

Theoretical implementation on the receivers by integrating the flux vector potential of the element edges across a specified contour using (1) is first performed inside the APDL script language of ANSYS. This contour as in Fig. 3 needs to be pre-defined before meshing the air in the software tool so that the postprocessor can find the nodes path and perform the

The flux derivative in time is nothing more than the induced voltage (2) and when multiplied by the number of turns, the result is the total induced voltage in the coil. The accuracy of this modified model is up to within 0.5% after signal amplification while the computational time has been nearly halved (see case1 in Fig. 5). Modeling the receivers is no longer required and the advantage here is not only the reduction of computational time but the flexibility of the model to provide, with one computation, all the induced voltages of all possible combinations of receiver(s) at all position(s), shape(s), and orientation(s).

4. Volumetric Estimation Method

4.1 Finite Element Mesh

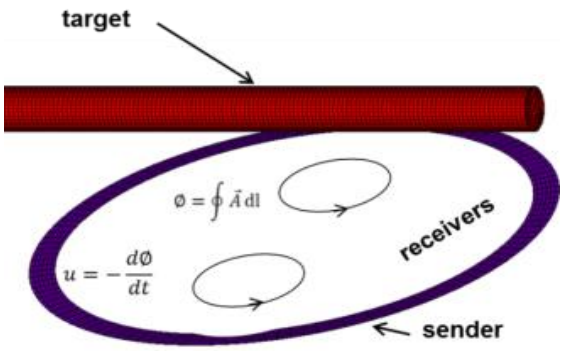

Fig. 3. Line receiver model

So far a complete full target has been modeled. Several checks are performed to see the accuracy versus computational time of several skin modification cases as in Fig. 4. If the magnetic flux is uniform and axial to a cylindrical target, for example, then it is assumed that eddy currents induced in the target are only circulating around the surface of this cylinder up to a depth of δ which is evaluated by (3) [10].

The target has an electrical conductivity σ and a magnetic permeability μ.

The excitation frequency f of the sender coil is also

included. Some published models take this estimation into account, such as the 'Thin Skin Approximation' (TSA) [7]. In order here to check the skin model, seven cases (Fig. 4) were checked and compared to a full complete model (complete coils and complete target is case 0). This means cases 1 to 7 all use the "Line Receiver Model" described in section III for the calculation of the induced voltage of the receivers. Case 1 has the same target model as Case 0. Case 2 models only the skin, with 3 layers of total height δ which is computed from (3) but this time without the core of the target. Case 3 models the skin depth with only two layers.

TABLE 1. Response of the seven cases compared to the complete model (case 0)

Case	Amplitude [db]		Relative accuracy to case0 [%]	
	100kHz	200kHz	100kHz	200kHz
0	61.63	55.25	0.00	0.00
1	62.30	55.88	1.09	1.14
2	62.91	56.49	2.08	2.24
3	58.45	52.7	-5.16	-4.62
4	58.04	52.18	-5.83	-5.56
5	59.03	53.16	-4.22	-3.78
6	62.93	56.49	2.11	2.24
7	62.2	56.06	1.44	1.47

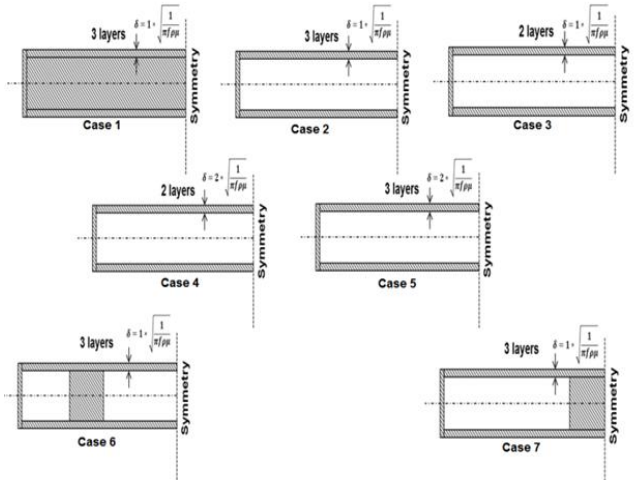

Fig. 4. Seven different skin designs to be compared to the complete model

Cases 4 and 5, model twice the skin depth with two and three layers respectively. Cases 6 and 7 are the same as case 2 but a small part of the core (10mm axially) is kept due to the fact that the eddy current distribution is not uniform in the target. For that reason, the most accurate approximation (referring to Table 1) relative to the complete model (case 0) is case 7 which is also one of the most efficient concerning computational time as shown in Fig. 5. a computational harmonic model

$$\delta = \sqrt{\frac{1}{\pi f \sigma \mu}} \tag{3}$$

about ten times faster has been realized with up to 1% accuracy relative to the complete model. As a conclusion, modeling only the skin, as in TSA [7] for example is sometimes not very accurate because of finite target shapes and its relative position to the sensor. Not only that eddy currents may flow locally in the core part of the cylinder but also the inductance of the system may not be preserved if one models only the skin. For this reason, a volumetric approximation method is needed to automatically predict the current density distribution in the target from the time derivative of the vector potential, thus preparing the exact mesh requirement before finalizing the simulation procedure of all system parameters.

4.2 Volumetric Estimation Method

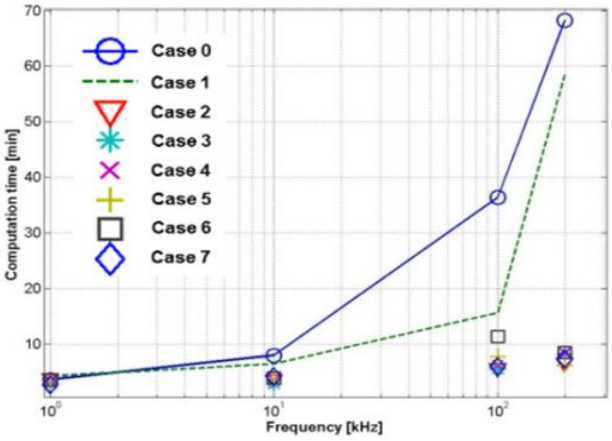

Fig. 5. Computational time of all cases relative to Case

According to Fig. 5 the most efficient cases in reduction of computational time were the ones with less target elements. The target elements have additional electric degrees of freedom (DOF) and any reduction in these elements would contribute highly in having fast computations. When models are computed in transient 3D solvers, the computational time may be unbearable. One part of the current work is an instantaneous prediction of high current densities in the target at time step {n+1} from known values of vector potential derivatives at time step {n}.

Deriving the second Maxwell's equation as in [11], (4) states that a change in the magnetic field leads to an electric field in a conductive target.

$$\nabla \times \{\vec{E}\} = -\left\{\frac{\partial \vec{B}}{\partial t}\right\} \tag{4}$$

$\{\vec{E}\}$ = electric field intensity vector

$\{\vec{B}\}$ = magnetic flux density vector

And rewriting it in terms of magnetic vector potential {A} will lead to (5)

$$\vec{J_e} = -\frac{1}{\rho}\left\{\frac{\partial \vec{A}}{\partial t}\right\} \quad (5)$$

$\{\vec{J_e}\}$ = induced eddy current density vector

$\{\vec{A}\}$ = magnetic vector potential

ρ= electric resistivity

The induced eddy current density can be estimated from the time derivative of the vector potential which in turn is a degree of freedom in the transient finite element solver. Making use of (5) one already has information where are the possible locations of eddy currents in a conductive target in the next time step. In order to realize this, a simple pulse induction of a metallic sphere is setup.

4.3 Pulse induction of a metallic sphere

The coil is excited with a constant voltage to reach a steady state and then switched off and let the current in the coil diminish to zero very fast in time. The same coil is used here as a sender and receiver.

The sphere radius is 4mm and a simple check of the two quantities of (5) for the three different materials confirms that steel1 & steel2 do not need the complete radial space as for the case of copper. Fig 7 shows that 2μs after the pulse is activated, the current density J can be neglected between the center (0mm) and 3mm distance from the center. After 25 μs the complete sphere is active and thus the core radial limit is 0mm as shown. While for steel the inner core of the sphere (0mm to ~2.5mm) is still not active even after 45 μs. steel2 is four times more permeable than steel1; that's why the active skin depth is nearly always about two times thinner than the skin of steel1. This means at 25 μs., for example, the steel1 inactive core is 3mm (1mm skin) while steel2 is3.5mm(0.5mm skin) which proves the physicality of (5). The main observation of Fig. 7 is that for each of the three materials the radial limit of $-\frac{1}{\rho}\left\{\frac{\partial \vec{A}}{\partial t}\right\}$ is always lower than the limit of $\vec{J}_e$ at any given time. In other words the radial limit of inactive sphere core predicted by $-\frac{1}{\rho}\left\{\frac{\partial \vec{A}}{\partial t}\right\}$ at time "t" is the same as $\vec{J}_e$ at time "t+Δt". This criteria allow predicting the future space limit of the current density derived from the actual vector potentials present in the database history of an FEA simulation solver.

4.4 Simulation Results

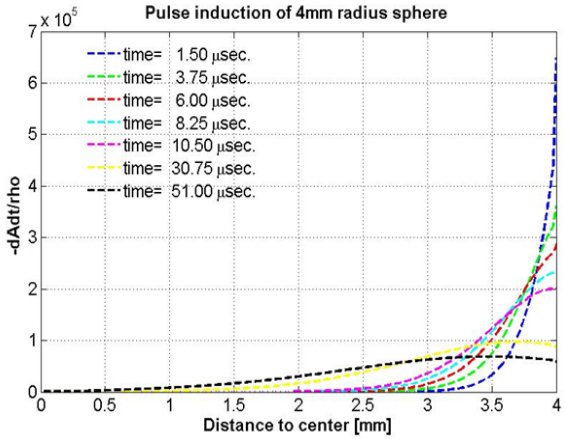

Fig. 8. Instantaneous plots of vector potential derivative across the radius of the copper sphere

Quantifying what is described before, Fig. 8 and 9 both show the difference between copper and steel by plotting the term $-\frac{1}{\rho}\left\{\frac{\partial \vec{A}}{\partial t}\right\}$ across the sphere radius. At the first microseconds after the pulse there will be a jump in the current density at the skin. But after that the field diffuses to the inner core of the sphere. In the case of steel, this diffusion is limited and even after 50 μs (black curve in Fig. 9) the limit of 3 mm (1 mm skin) is reached in contrast to copper where the whole sphere is occupied. That's why when applying a space reduction procedure then the unnecessary finite elements that can be eliminated at around 41 μs. (see Table 3) are much more than the ones for copper.

Referring to the current density plots between copper and steel in Table 3 one notices clearly the instantaneous distribution and its transient reduction of elements. This kind of automatic moving skin depth has one drawback which is when the core limit is

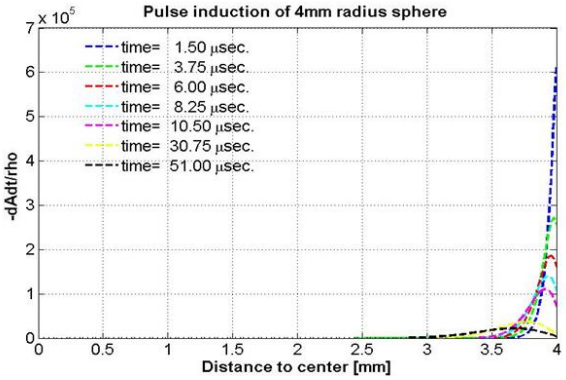

Fig. 9. Instantaneous plots of vector potential derivative across the radius of the copper sphere

overestimated, or the skin is underestimated, the border

current density may not be low and needs to be corrected before the next time step is solved. For that reason a slight modification is implemented by using (5) again and taking the derivative of both sides. And since the sphere is assumed to be fixed in space the only variable is time then this leads to (6).

$$\frac{d\vec{J_e}}{dt} = -\frac{1}{\rho}\left\{\frac{d^2\vec{A}}{dt^2}\right\} \qquad (6)$$

(6) is helpful when discretized in time to estimate $-\frac{1}{\rho}\left\{\frac{\partial\vec{A}}{\partial t}\right\}$ at a certain location in space and at time "t+Δt" from values at time "t" or simply suggest the speed of the diffusion of current density inside the core of the sphere and thus the next corrected border limit.

As a summary of the results one can state that modeling a permanently fixed skin depth is not always accurate during a transient simulation. On the contrary, the proposed 'moving skin depth' procedure allows a future prediction of the possible current density location.

TABLE 3. FEA Mesh and Current Density

	0 µs	7 µs	21 µs	41 µs	200 µs	400 µs
copper Mesh						
steel 1 Mesh						
copper Jz						
steel 1 Jz						

he disadvantage of finite element elimination from the target core is a sudden change in the effective inductivity of the system. For copper with relative permeability unity this may not be a problem but for steel this can affect the accuracy of the results. If the aim of the simulation is to estimate the instantaneous Joule heat generated in the target then just eliminating the elements during the computational transient run is not enough. Rather would be more suitable in this case is to replace these elements by a material which has the same permeability but no resistivity. Calculation time will be a bit more than no elements at all but still less than having both degrees of freedom, electric and magnetic, present in these elements. Fig. 10 plots, for the three different materials, the flux density at the sphere surface (a) and the Joule heat of the complete sphere (b). The element reduction method is not acceptable while the DOF method is matching exactly with the complete model.

If the aim of the simulation is just to estimate the current density then Fig. 11 shows that even the element reduction method is not that far from the complete model.Planar simulations (infinitely long coils and cylinder target) were also checked and the same conclusions were drawn. The effect of these two methods may not be that high on the reduction of computational time in the case of 2D because the post processing of every time step is required to apply material change or element reduction and this may take the same time as the time saved in computation, but in 3D this will for sure be a great win.

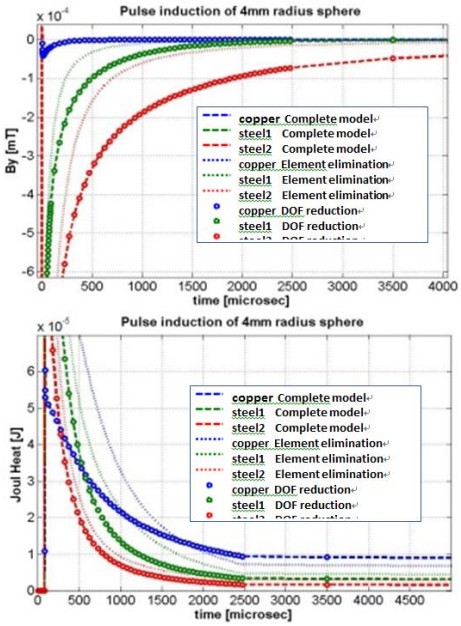

Fig. 10. a) up, Flux Density at the surface of the sphere with different material, b) bottom, Joule Heat of the complete sphere with different material using different methods

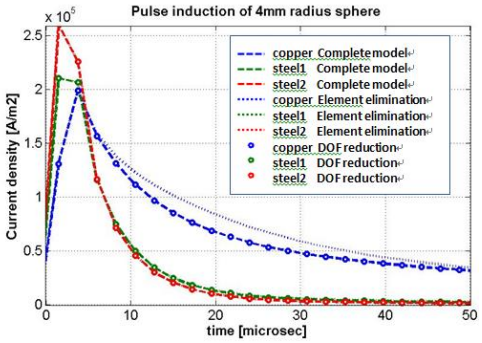

Fig. 11. Current density at the surface of the sphere with different material using different methods

4.5 Future work

Volumetric estimation method works fine for 2D and needs to be implemented in 3D. It uses the vector potential time derivative across arbitrary 3D target shape in arbitrary space direction to predict arbitrary surface border limits

starting from the skin inwards. This automated method will reduce the computational time significantly and still keep the highest accuracy possible.

5.Conclusion

A 'Line Receiver Model' that replaces classical modeling of induction PCB coils receivers with an accuracy of about 1% of the amplified signal is achieved and verified. The advantage (besides computational time reduction) is the ability to post-process the induced voltage for any receiver shape and location without the need to solve it again. In addition to that, an automatic instantaneous modification on the target body elements reduces computational time. This 'Volumetric Approximation Method' is based on locating the magnetic vector potential variation in time from previous time steps in the target and thus, adaptive finite element mesh is performed during transient FEA simulations. As a result, a final modified model with acceptable accuracy offering speed and robustness for future optimization of detection devices based on EMI is used and will be implemented in general 3D future applications.

References

[1] W. Chen, G.S. Zhang, Y.S. Sun, M.J. Chen, "Integrated Third Kind Boundary Condition for 2D eddy current problems and its application in NDT," *IEEE*, 1993

[2] A. Bernieri, G. Betta, L. Ferrigno, "Characterization of a magnetic measurement system for NDT," *IEEE Transactions on Instrumentation and Measurement*, 2002

[3] Y. Das, J. E. Mcfee, R. H. Chesney, "Time domain response of a sphere in the field of a coil: theory and experiment," *IEEE Transactions on Remote Sensing and Geoscience* , 1984

[4] J. W. Luquire, W. E. Deeds, C. V. Dodd, "Axially symmetric eddy currents in a spherical conductor," *Journal of Applied Physics*, 1970

[5] W. Renhart, C. Magele, "Optimal design of a coil arrangement for the identification of hidden ferrous objects," *IEEE Transactions on Magnetics*, 2002

[6] K. O'Neill, K. Sun, C.C. Chen, F. Shubitidze, K.D. Paulsen, "Combining GPR and EMI data for discrimination of multiple subsurface metallic objects," *IEEE*, 2003

[7] C. D. Moss, K. O'Neill, T. M. Grzegorczyk, J. A. Kong1, "A hybrid time domain method to calculate electromagnetic induction scattering from targets with arbitrary skin depths,"

[8] A Langman, M.R. Inggs, "A stepped frequency CW polarimetric radar for mine detection," *IEEE*, 1996

[9] D.Vasic, V. Bilas, D. Ambrus, "Pulsed eddy current nondestructive testing of ferromagnetic tubes," *IEEE*, 2004

[10] I.J. Won, D. Keiswetter, "Electromagnetic induction spectroscopy," *SPIE Conference on Detection and Remediation Technologies for Mines and Minelike Targets*, 1998

[11] W. R. Smythe. Static and Dynamic Electricity. *McGraw-Hill Book Co, New York, NY.* 1950.

Chafic Abu-Antoun received his M.Sc. in mechanical engineering in 2002 from Univer sity of Balamand, Lebanon. After that he wo rked in Germany and pursued in parallel to h is job a M.Sc. degree in Computational Scie nces from Stuttgart University in 2007. Sinc e then he works as a research engineer in Hil ti AG, Liechtenstein. His fields of interest are electromecha nical actuators and motors, electromagnetic sensors, and ind uction heating. Since

Yves Perriard is born in Lausanne in 1965. He received the M. Sc. in Microengineering from the Swiss Federal Institute of Technology - Lausanne (EPFL) in 1989 and the Ph.D. degree in 1992. Senior lecturer from 1998 and professor since 2003, he is currently director of the Integrated Actuator Laboratory at EPFL. His research interests are in the field of new actuator design, new magnetic liquid and associated electronic devices. In 2014 he is appointed guest professor at Zhejiang University in China. He is author and co-author of more than 150 papers and patents.